Journal of Material Cycles and Waste Management (2022) 24:949–970
https://doi.org/10.1007/s10163-022-01369-x

ORIGINAL ARTICLE

Utilization of alum sludge waste for production of eco-friendly blended cement

O. A. Mohamed[1] · S. M. A. El-Gamal[2] · A. A. Farghali[3]

Received: 18 September 2021 / Accepted: 31 January 2022 / Published online: 18 February 2022

Abstract

This work was focused on evaluating the suitability of replacing Portland cement (PC) by 5, 10 and 15 mass % of activated alum sludge waste (AAS) as a pozzolanic material. Exploitation of low-cost nanocomposite for bolstering the physical, mechanical, and stability against firing of PC–AAS-hardened composites was inspected. $CuFe_2O_4$ spinel nanoparticle with average particle size (~ 50 nm) was prepared. Inclusion of $CuFe_2O_4$ spinel in different PC–AAS-hardened composites bolsters their physicomechanical features at almost normal curing ages as well as their stability against firing. The positive impact of synthesized $CuFe_2O_4$ spinel was affirmed via TGA/DTG and XRD techniques, which indicated the presence of diverse hydration yields such as CSHs, CASHs, CFSH, and CuSH that enhance the overall physicomechanical characteristics and thermal stability of various PC–AAS-hardened composites. The composite containing (90 PC–10 AAS waste–2 $CuFe_2O_4$) offers many benefits from the economic and environmental view.

✉ O. A. Mohamed
Ola.abdelaziz.mohamed@psas.bsu.edu.eg

[1] Environmental Science and Industrial Development Department, Faculty of Postgraduate Studies for Advanced Sciences, Beni-Suef University, Beni-Suef 62511, Egypt

[2] Chemistry Department, Faculty of Science, Ain Shams University, Cairo, Egypt

[3] Materials Science and Nanotechnology Department, Faculty of Postgraduate Studies for Advanced Sciences (PSAS), Beni-Suef University, Beni-Suef 62511, Egypt

Graphical abstract

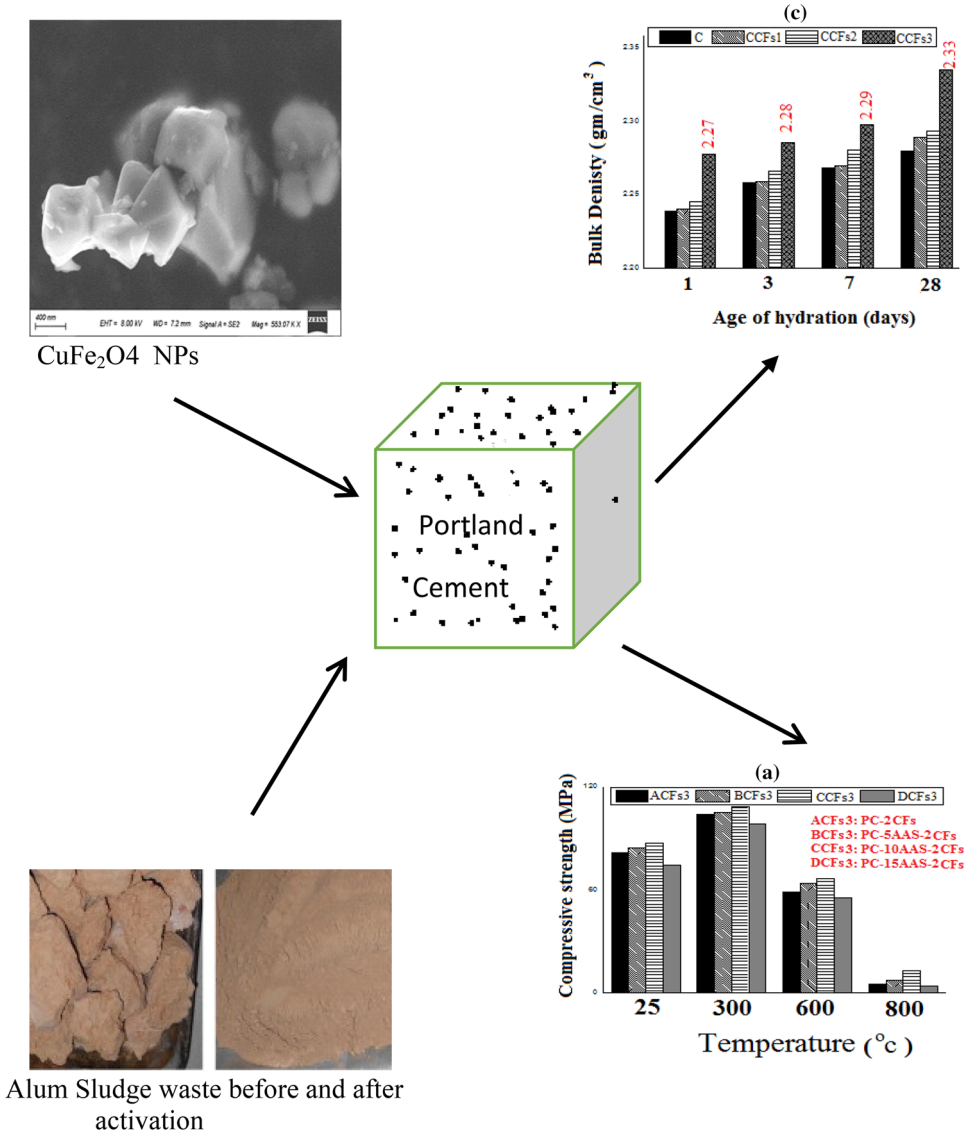

Keywords $CuFe_2O_4$ spinel · Activated alum sludge · Stability against firing · Morphological features

Introduction

Alum sludge (AS), a by-product of water treatment plants, is considered hazardous waste and the conventional disposal by landfill is not feasible. The disposal of solid wastes, especially alum sludge (AS), has become urgent to minimize environmental threats [1–3]. However, treated alum sludge (TAS) possesses high contents of SiO_2 and Al_2O_3, which are the fundamental constituents of cement. So, the feasibility of reusing AS, as a pozzolanic material, with Portland cement (PC) due to their capacity for reacting with calcium hydroxide formed during the hydration of PC has gained interest among concrete researchers [4]. Recently, few studies have investigated the feasibility of using calcined water treatment sludge (WTS) as supplementary cementitious material in cement-based materials due to high pozzolanic activity and evaluated its influence on the mechanical properties of cement. The results indicated that the inclusion of drinking water sludge ash (DWSA) with Portland cement induced the formation of aluminum-bearing hydrates, such as ettringite and calcium aluminate hydrates (C–A–H) [5–7].

Over the past few years, nanotechnology was utilized widely in almost all fields of our life to provide novel applications, especially in the construction sector. Nanoparticles'

incorporation to cement materials to inspire new types of building materials with high efficiency and resistance under drastic environmental conditions used in diverse applications are being devoted much attention [8, 9].

Nano silica, nano iron, nano alumina, nanofibers, nano titania, and carbon nanotubes are the most widely used nanoparticles [10–13]. Ferrites are one of the most basic components in the electronic industry; ferrite is used in many applications, including rotary transformers, noise filters, and multilayer ferrite chip components because of its magnetic semiconductor properties [14].

Recently, the impact of Fe_3O_4 spinel nanoparticles on the durability of cementing materials was investigated; the results revealed that spinel nano-Fe_3O_4 enhances their thermal stability and the resistivity against aggressive anions present within the matrix [15].

Many researches have been reported, as mentioned previously, to investigate the effect of nanoparticles on the different characteristics of cementitious matrices, but there are no/and or rare studies investigating the effect of $CuFe_2O_4$ spinel nanoparticles. Consequently, this study aimed to utilize low-cost synthesized $CuFe_2O_4$ spinel nanoparticles (CFs NPs) as an additive for boosting the mechanical properties and fire resistivity of hardened pastes made from ordinary Portland cement replaced by various ratios of activated alum sludge and investigating the feasibility of the reuse of activated alum sludge for partially replacing Portland cement in construction materials, which help in minimizing the environmental threats, as well as contribute to solving the environmental and economic problems faced by Portland cement production.

Experimental program

Materials

Portland cement (PC-type I) has a Blaine surface area of 3495 cm^2/g. Cement used in this study was delivered from El-Sewedy cement group, Al-Ain Al-Sokhna, Suez, Egypt. Water treatment plant sludge waste (WTPS) was produced from processes for purifying drinking water. The (WTPS) used in this research was collected at the Beni-Suef water treatment plant. The WTPS was dried in an oven at 105 °C for 24 h and then crushed. In this study, alum sludge was thermally activated via firing the dry WTPS in an electric furnace at 500 °C for 2 h and then cooled gradually to room temperature. The XRD patterns of activated alum sludge waste (AAS) after calcination at 500 °C are clarified in Fig. 1. The chemical oxide compositions of PC, mineralogical phase compositions of PC, and oxide composition of AAS are given in Table 1.

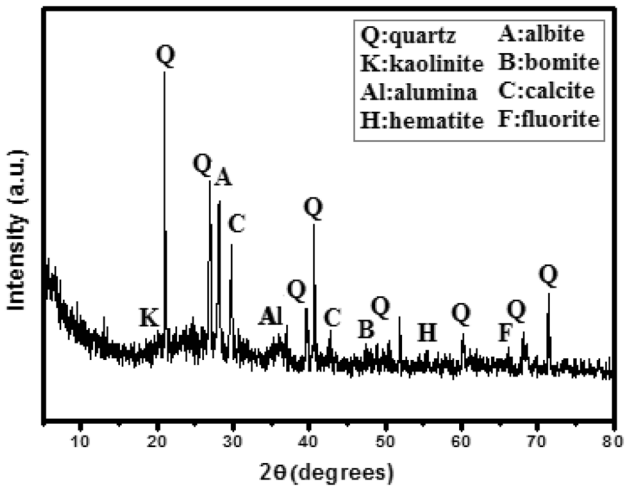

Fig. 1 X-ray diffraction patterns of activated alum sludge waste (AAS) after calcination at 500 °C

Table 1 Chemical oxide compositions of raw materials

Oxides	PC (mass %)	Sludge (mass %)
CaO	62.3	6.80
SiO_2	19.2	62.64
Al_2O_3	4.9	13.66
Fe_2O_3	3.6	5.00
MgO	2.44	1.50
SO_3	2.8	0.65
Na_2O	0.41	0.48
K_2O	0.63	0.76
Cl^-	0.09	0.182
LOI	3.63	
LSF	–	3.94
Mineralogical phase composition of PC (mass%)		
C_3S	51.52	
C_2S	16.26	
C_3A	6.95	
C_4AF	10.96	

The pozzolanic activity of activated alum sludge waste (AAS) was evaluated according to the TS 25 standards [16] through the compliance with the chemical and physical requirements of standards applicable to normal pozzolanic material, where the TS 25 standard [16] suggests that $SiO_2 + Al_2O_3 + Fe_2O_3$ should be at least 70%, $SO_3 \leq 3.0\%$, $CI^- \leq 0.1\%$, and the reactive silica content of pozzolanas $\geq 25\%$. The XRF analysis of AAS as presented in Table 1 emphasizes the capability of using activated alum sludge waste (AAS) as supplementary cementitious materials (SCM) with properties equivalent to those of a normal active pozzolanic material [17].

Table 2 Physical properties of polycarboxylate super plasticizer (SP)

Appearance	Yellow-brown liquid
Solid residue (%)	39.9%
pH	7.51–7.53
Specific gravity (g/ml)	1.08

The superplasticizer (SP) used in this study is a modified polycarboxylate-based superplasticizer (PCsp) (Sika Viscocrete 5230 L) with a specific gravity of 1.08 g/ml, supplied from Sika Company, Elobour City, Egypt. SP superplasticizer is used as a dispersing agent for the nanoparticles, as well as to achieve the desired workability of different pastes [18]. Some physical properties of SP superplasticizer are given in Table 2.

Using commercial types of reagents and starting materials to mitigate the economic cost, $CuFe_2O_4$ spinel nanoparticles (CFs NPs) with nanoparticle size ~ 200 nm was synthesized according to the previously reported method as follows: two moles of pure fine powder ferric acetate basic ($(CH_3COO)_2$ Fe·OH) were well mixed in a ball mill for 6 h with 1 mol of copper (II) acetate monohydrate ($(CH_3COO)_2$ Cu·H_2O) to ascertain the homogeneity. The mixture was then dried at 150 °C and the sample was heated on a hot plate to facilitate decomposition of acetates, then fired at 1000 °C for 2 h to obtain copper ferrite nanocrystals. CFs NPs with average particle size ~ 50 nm were obtained by mechanochemical degradation of the obtained 200 nm CFs NPs. This was achieved by ball milling for 40 h, followed by gradual heating in a muffle furnace up to 500 °C for 2 h. The obtained CFs NPs (50 nm) have saturated magnetic flux density (Bs) value 39.1 emu/g, remnant magnetic flux density (Br) 4.002 emu/g and high coercivity (Hc) value 85.56 Oe [19]. HR-TEM, SEM/EDX, XRD, and N_2-adsorption/desorption analyses of CFs NPs are clarified in Figs. 2, 3, 4, 5. Elemental chemical analysis of the prepared $CuFe_2O_4$ nanocomposite was determined by energy-dispersive X-ray (EDX) analyzer using Bruker nano detector attached to SEM. The data confirmed that it has a purity of ~ 99.0%. Obviously from the results displayed in Fig. 3, the sample contains only copper, iron and oxygen and the atomic percentage is almost close to the stoichiometry; 1:2:4 ratios for Cu:Fe:O, respectively. Also, there is no trace of impurities detected, which confirms the phase purity of the samples [20].

Table 3 illustrates some important characteristics of $CuFe_2O_4$ spinel nanoparticles (CFs NPs).

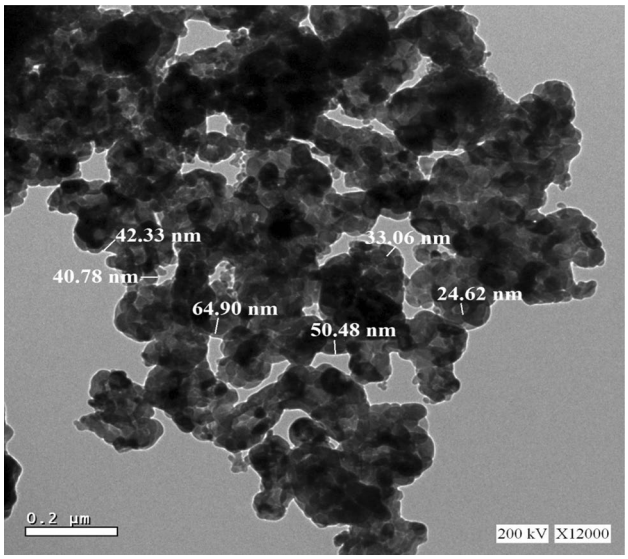

Fig. 2 HR-TEM of $CuFe_2O_4$ nanoparticles

Methods and techniques

Different groups of PC–AAS dry mixes were prepared, and their composition and designations are presented in Table 4. Each dry cement blend was mechanically mixed in a porcelain ball mill for 8 h to assure complete homogeneity of the dry mixture. Various additions of (CFs NPs) were utilized to improve the pastes of different blends. CFs NPs were added to the superplasticizer aqueous solution (containing 0.30% of SP by mass of solid) using the total amount of mixing water and the resultant suspensions were sonicated at 25 °C for 1 h. Pastes for different tests were prepared by mixing the dry mixes with 0.27 water/cement ratio.

Pastes of different mixes were prepared by mixing the dry samples with the desired amount of water (containing the dispersed CFs NPs in case of nanocomposites preparation), and the mixing process continued for about 4 min to form each paste. Cubic specimens (2.5 × 2.2.5 cm) of each paste were prepared using cubic molded galvanized steel. The fresh molded pastes were kept at ~ 100% relative humidity for 1 day to achieve the final setting. Then, the cubic specimens were left under tap water at room temperature for 3, 7, and 28 days. Ton-industrie machine (West Germany) was used for compressive strength test; the average value of the three cubes was recorded each time. The hydration reaction of the shattered specimens was stopped using stopping solvent prepared from methanol–acetone mixture (1:1 by volume) according to the previously reported method [21]. The produced samples were left at 75–80 °C for 3 h and then maintained in a desiccator (containing soda lime and $CaCl_2$) until the time of testing was reached.

Some important physical properties were followed via assessments of total porosity (TP), bulk density (BD), and water absorption (WA) values at definite time intervals According to ASTM (C140 and C150) [22]. Equations 1, 2, and 3 are used to calculate BD, TP, and WA, respectively.

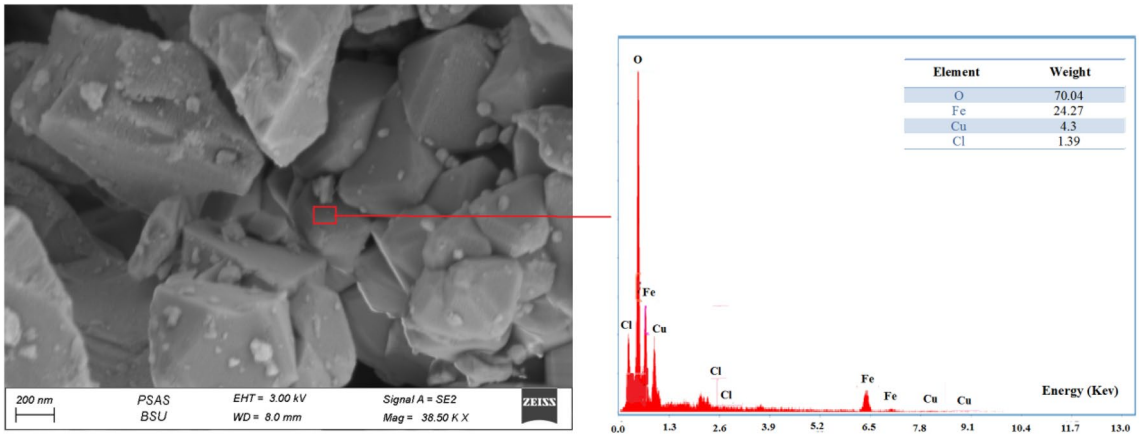

Fig. 3 SEM/EDX images for $CuFe_2O_4$ nanoparticles

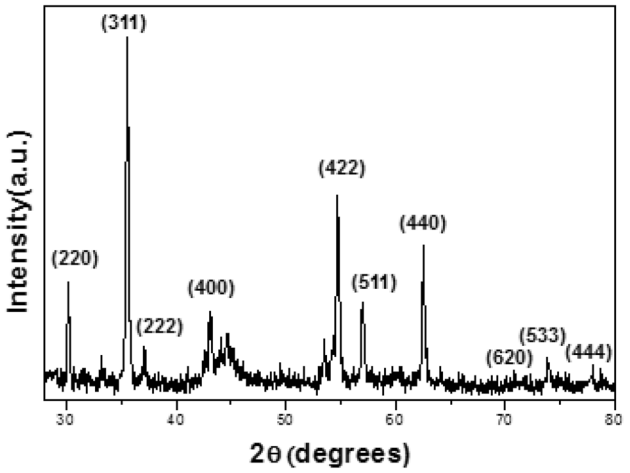

Fig. 4 X-ray diffraction patterns of copper ferrite nanoparticle $CuFe_2O_4$

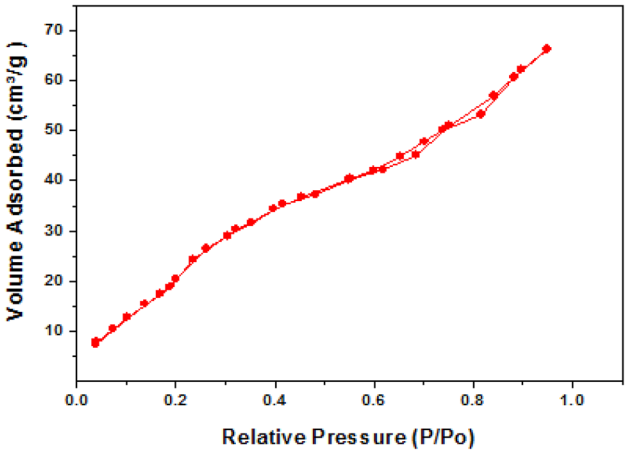

Fig. 5 N2-adsorption/desorption isotherm of CFs NPs

$$\mathrm{BD}\ \left(\mathrm{g/cm^3}\right) = \frac{\mathrm{W3}}{\mathrm{W1} - \mathrm{W2}}, \tag{1}$$

$$\mathrm{TP}\ \% = \frac{\mathrm{W1} - \mathrm{W3}}{\mathrm{W1} - \mathrm{W2}} \times 100, \tag{2}$$

$$\mathrm{WA}\ (\%) = \frac{\mathrm{W1} - \mathrm{W3}}{\mathrm{W3}} \times 100, \tag{3}$$

where W1, W2, and W3 are the weights of saturated, suspended, and dried (at 105 °C overnight) samples, respectively.

The samples used for the thermal stability test were treated for 28 days under water, dried at 80 °C for 1 day, and then fired at 300, 600, and 800 °C for 3 h. The fired samples were cooled in two ways: the first group of specimens was left to cool gradually, while the second group cooled rapidly by immersing in tap water. The compressive strength was measured for each set of cooled specimens [23].

X-ray diffraction (XRD), thermal gravimetric analysis (TGA/DTG), and scanning electron microscopy (SEM) techniques were applied for some selected specimens to identify the textural properties and phases formed during the hydration process.

Results and discussion

Physicomechanical aspects

Compressive strength (CS)

The mechanical properties of the treated specimens were evaluated via the determination of the compressive strength (CS) values at different periods of hydration. The CS values

Table 3 Some properties of the synthesized CuF_2 O_4 spinel nanoparticles

Crystallite size (nm)	Lattice parameter (Å)	S_{BET} (m^2/g)	Purity (%)	pH	Remnant magnetic flux density B_r (emu/g)	Saturated magnetic flux density B_s (emu/g)	High coercivity H_c (Oe)
50 ± 10	8.369	66	99	9	4.002	39.11	85.56

Table 4 Percentage composition and notation of different mixes

Mix	Mix proportions (mass %)				Water/cement W/C ratio
	PC	Sludge	(CFs NPs)	Superplasticizer	
A	100	–		0.30	0.27
ACFs1	100	–	0.5	0.30	0.27
ACFS2	100	–	1.0	0.30	0.27
ACFs3	100	–	2.0	0.30	0.27
B	95	5		0.30	0.27
BCFs1	95	5	0.5	0.30	0.27
BCFs2	95	5	1.0	0.30	0.27
BCFs3	95	5	2.0	0.30	0.27
C	90	10		0.30	0.27
CCFs1	90	10	0.5	0.30	0.27
CCFs2	90	10	1.0	0.30	0.27
CCFs3	90	10	2.0	0.30	0.27
D	85	15		0.30	0.27
DCFs1	85	15	0.5	0.30	0.27
DCFs2	85	15	1.0	0.30	0.27
DCFs3	85	15	2.0	0.30	0.27

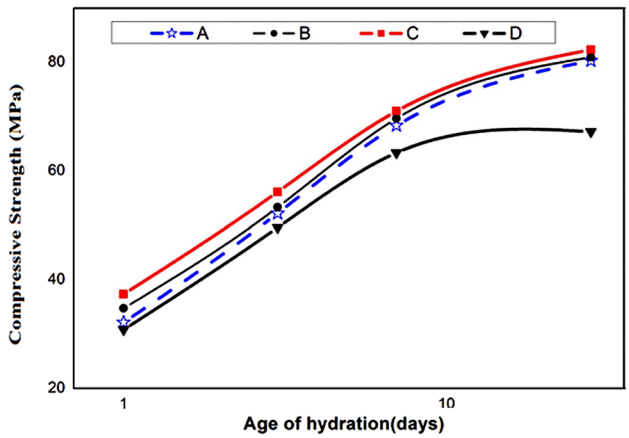

Fig. 6 Compressive strength versus age of hydration for hardened cement pastes (Mixes A–D)

of hardened composites prepared by replacing PC with 0, 5, 10, and 15% of activated alum sludge waste (AAS) (Mixes A, B, C, and D, respectively) are represented in Fig. 6. The CS values showed a general continuous development with an increasing hydration period for all tested mixes. In general, this continuous increase in the strength values is ascribed to the hydration of different phases present in Portland cement clinker and formation of hydration products mainly as (calcium silicate hydrates, C–S–H), (calcium aluminate hydrates, C–A–H), AFm (alumino ferrite monosulfate hydrate, $3CaO.(Al, Fe)_2O_3.CaSO_4.nH_2O$ and AFt (alumino ferrite trisulfate, or ettringite $C_6A\check{S}_3H_{32}$) and calcium aluminosilicate hydrate (C-(A)-SH) [24].

Pastes prepared by replacing PC with 5 and 10% of AAS (mass %) (Mixes B and C; respectively) recorded the highest compressive strength (values at each testing hydration time relative to the control (neat PC) paste (Fig. 6). The reported higher strength values for these composites are linked to the existence of excessive amounts of nearly amorphous and illcrystalline CSH as the main product, obtained via the pozzolanic interaction between AAS waste (alumina and silica phases) and calcium hydroxide, obtained from cement clinker hydration. These hydrates fill up the pores present along with the matrix as well as act as binding centers between the remaining present unhydrated grains.

On the contrary, by increasing the AAS waste to 15% (Mix D), the CS values become comparable or even lower after 28 days than that of blank (Mix A). This decrease in the CS can be ascribed to the dilution effect of PC as a result of its replacement with high percentages of AAS waste, which in turn reduces the amount of $Ca(OH)_2$ liberated as a secondary hydration product from C_3S and β-C_2S phases that required activating the AAS waste [25]. The CS results affirmed that the optimum replacement ratio of PC by AAS is 10%; this conclusion has been reported previously by many researchers [26].

Figure (7a–d) clarifies the effect of additions of 0.5, 1.0 and 2.0% CFs NPs on the CS values of neat PC pastes (Mixes ACFs1–ACFs3, BCFs1–BCFs3, CCFs1–CCFs3 and DCFs1–DCFs3). The addition of different doses of CFs NPs to PC or PC replaced by different masses of AAS waste promotes notable enhancement in the compressive strength values compared to those of their references (Mixes A–D) during all hydration intervals (Figs. 7a–d). These results are imputed to the nanoparticle characteristics of CF spinel, such as great specific surface area 66 m^2/g, nano dimension 50 nm and, finally, the good distribution of it along with the cement matrix that enables it to fill the nano- and micropores existing among different

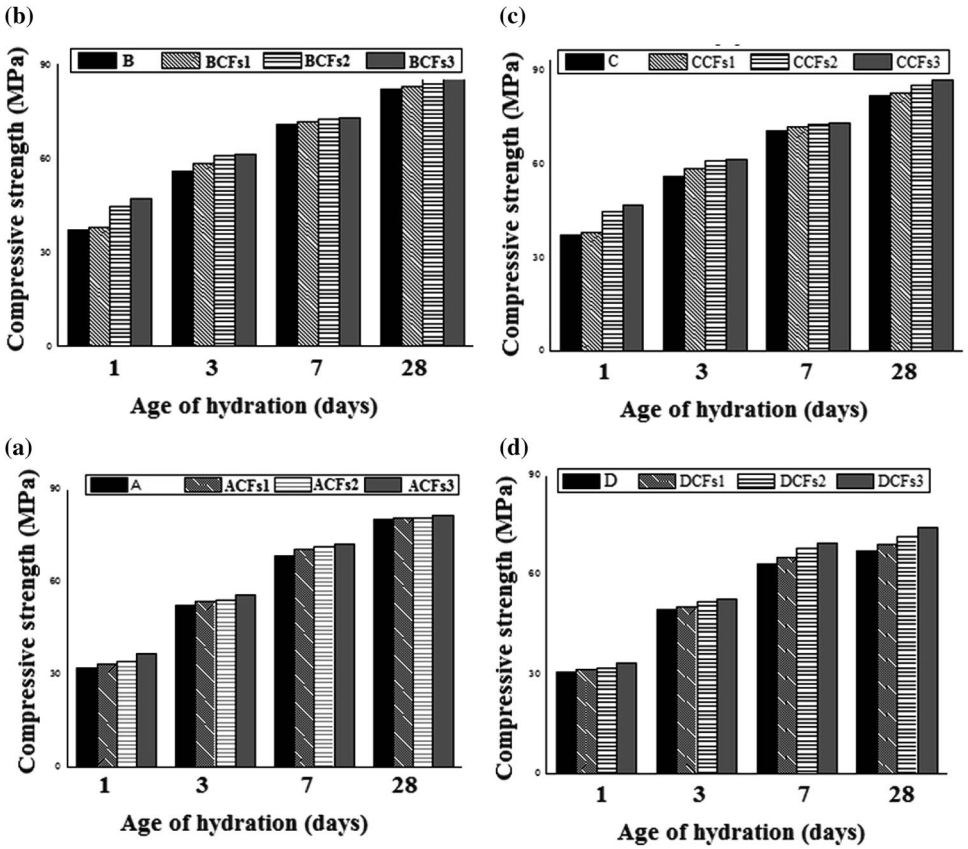

Fig. 7 Compressive strength values of different hardened cement composites

hydration products, giving rise to dense and compact structure with higher strength values than those of their control (Mix A). Besides, CFs nanoparticles act as active nucleation centers that accelerate the hydration process of cement grains to generate new and additional amounts of different hydrated phases, namely, CSHI (poorly crystalline foils or platelets which have a C/S molar ratio of 0.8–1.5), CSHII (fibrous structure with a C/S molar ratio of 1.5–2.0), calcium aluminate hydrates (C_3AH_6), calcium aluminosilicate hydrate (Ca-(A)-SH), and calcium ferrosilicate hydrate (like ilvaite, $CaFe^{2+}Fe^{3+}Si_2O_7O(OH)$, (CFSH)) [27].

As a general observation, as the amount of addition of CFs NPs increases (from 0.5 to 2%), its enforcement effect increases for all tested mixes, which is reflected as an increase in the CS values. This enhancement is ascribed to the filling effect of the CFs NPs that promoted reduction in the porosity of the cement matrix. Furthermore, the high alkalinity (pH ~ 12) of the composite matrix induced the partial ionization of CFs NPs into Cu^{2+} and ferric anion. These ions interact with $Ca(OH)_2$ in the presence of amorphous SiO_2 present in the AAS waste, generating an excessive amount of new hydrates [suchas copper silicate hydrate $Cu_2Si_2O_7(OH)_4.nH_2O$ (CuSH), calcium ferrosilicate hydrate (such as ilvaite, $CaFe^{2+}Fe^{3+}Si_2O_7O(OH)$, (CFSH)) that strongly participate in the upgrade of the CS values at all intervals of hydration [26]. These findings will be supported by the XRD analysis performed for some selected composites.

In conclusion, the results affirmed that 90% PC–10% AAS–2% CFs composite (Mix CCFs3) could be considered the optimum choice for general construction application, as it displayed the highest CS values as compared to all other tested nanocomposites at almost all testing ages. Undoubtedly, from the economic and environmental point of view, this composite (90PC–10AAS–2 CFs) offers many benefits, as replacement of PC by 10% AAS helps in reducing waste disposal costs (landfill tax), offering an alternative use for recycled water-treated plant sludge, without prejudging on either cost or quality as well as protecting the environment by saving energy and diminishing the amount of harmful gases (CO_2 and NO_x) and other air pollutants emitted from the cement industry.

Bulk density

The results of bulk density (g/cm^3) of various mixes are graphically represented in Fig. 8a–e. The bulk density (BD) values indicate a continuous increase from 1 to 28 days of hydration for all the tested composites. These findings could be ascribed to the stuffing of pores over time with the accumulated hydration products, which

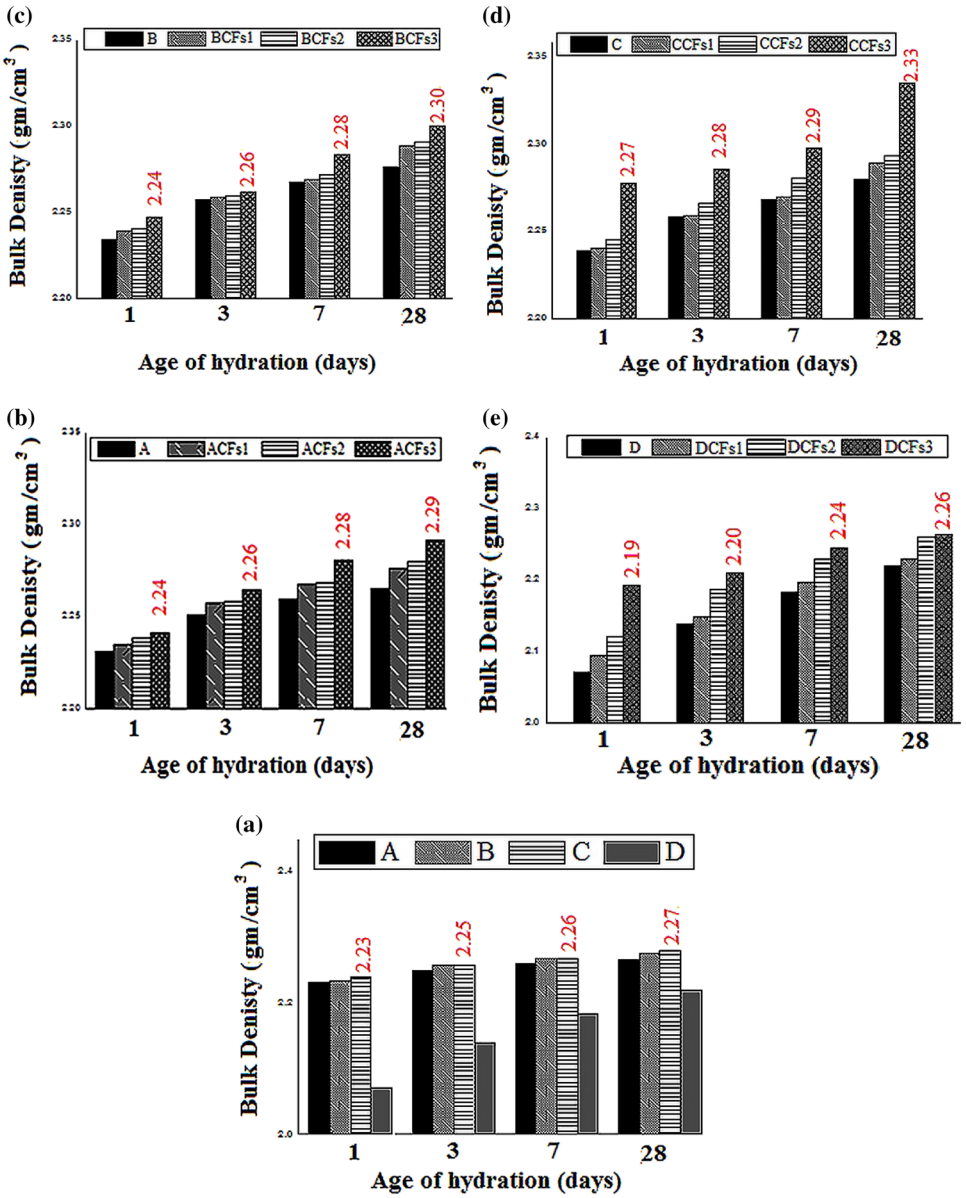

Fig. 8 Bulk density values of all hardened composites

promoted the formation of a dense and compact structure. Figure (8a) reveals that the BD values of Mixes B and C are higher and/or comparable to that of blank (Mix A), while the BD values of Mix D are lower and/or comparable to the control (Mix A). These results are in agreement with the CS results. The increase in the BD values in the case of composites made from Mixes B and C is assigned to the excessive amount of hydration products formed from the pozzolanic reaction between calcium hydroxide, liberated from cement clinker hydration, and AAS waste as mentioned previously. These products are stacked in most of the available spaces (pores) along the hardened cement matrix, promoting depletion in the total porosity (as will be discussed) and raising the BD values of the hardened composites. In the case of composite made from Mix D, the additionally formed hydration products from the pozzolanic interaction between the available CH and AAS are less than in the case of Mixes B and C for the previously mentioned factors mentioned in the compressive strength section. So, this mix showed DB values lower than (Mixes B and C), but still comparable to that of the blank (Mix A). The main observation is that the bulk density values of hardened nanocomposites (containing CFs NPs) are higher than that of their control (Mixes A, B, C, and D), and the densification effect (high bulk density values) increases as the CFs NPs content increases Fig. 8b–e. This finding is certainly owing to the activation impact of CFs NPs, as CFs act as foreign nucleation centers that accelerates the hydration process and promotes the formation of an extra amount of C-S-H gel [calcium silicate hydrate

($3CaO.2SiO_2.3H_2O$], CASH, CAH [calcium aluminate hydrate $3CaO.Al_2O_3.6H_2O$], CFSH [calcium ferrosilicate hydrate, such as ilvaite, $CaFe^{2+}Fe^{3+}Si_2O_7O(OH)$], and copper silicate hydrate $Cu_2Si_2O_7(OH)_4.nH_2O$ (CuSH). These extra products are accumulated in the available pore-forming more compact and dense structure with higher BD.

Total porosity

The results of total porosity for different composites are represented in Fig. 9a–e. As Fig. 9a displays, the values of TP% showed a gradual decrease with the progress of the hydration process (from 1 to 28 days) for (Mixes A–D). This dwindling is assigned to the stacking of different hydrates

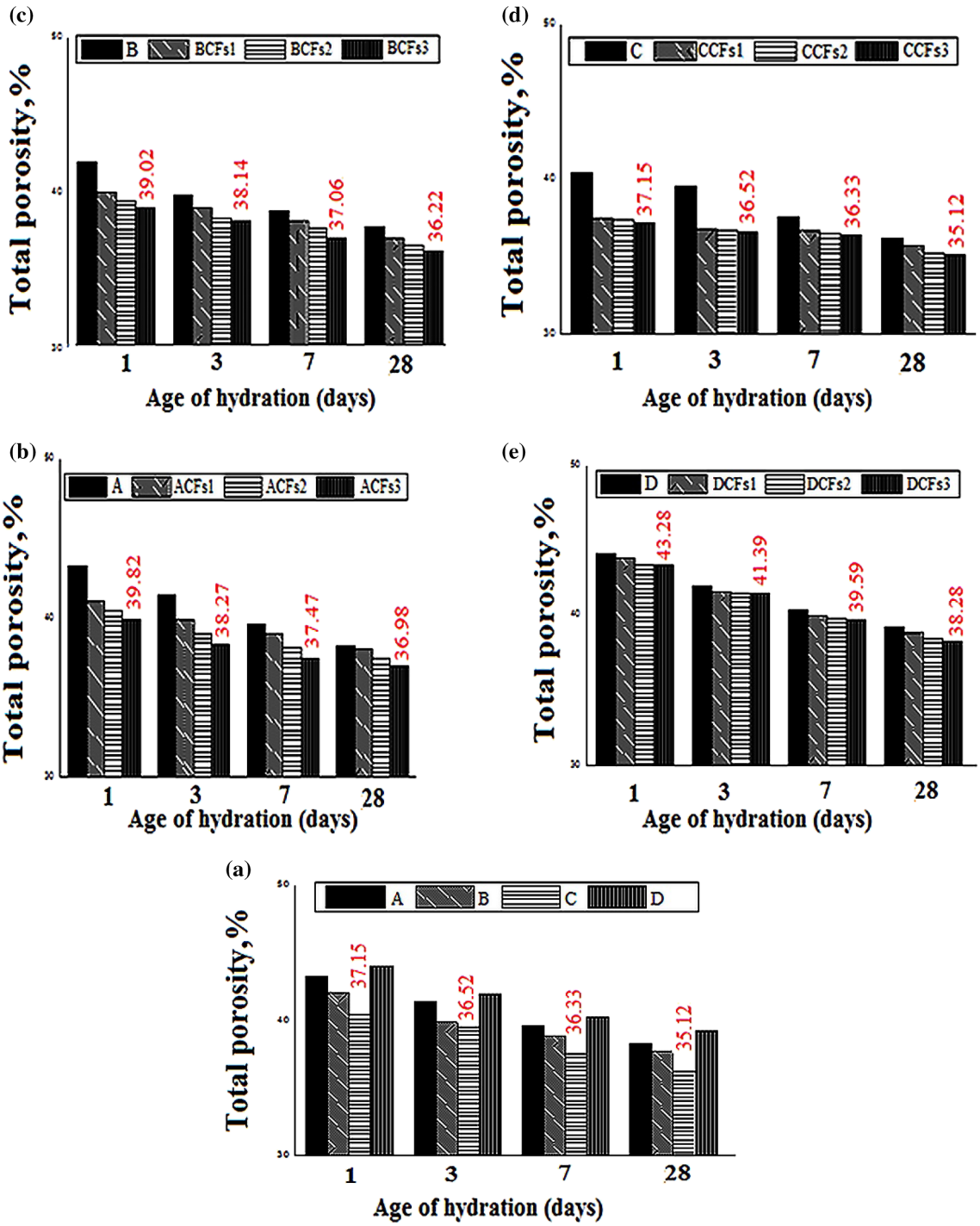

Fig. 9 Total Porosity values of all hardened composites

formed within the available spaces along with the composite matrix. Also, the TP values for (Mixes B and C) are lower than that of the control (Mix A), while for Mix D its TP values are comparable to the blank. These results are correlated with the BD and CS results and the explanation has been previously mentioned in these sections. Moreover, the presence of CFs NPs promoted a notable reduction in the total porosity for all prepared nanocomposites as compared to their control, and as the admixing amount of CFs increases, the reduction in the TP % increases Fig. 9b–e. The decrease in the TP % by the incorporation of CFs NPs is ascribed to the reduction in the available pores present along with the hardened matrix, owing to the CFs NPs acting as a filler as well as an activator that promote the formation of an extra amount of hydration products (namely: C–S–H gel, CASH, CAH, CFSH, and CuSH) that fill up the majority of the present pores.

Water absorption

Figure 10a displays the water absorption data obtained for Mixes A–D. The outcomes of this test are: (1) WA values of all tested composites decreased with curing age; (2) blended composites made from Mixes B and C displayed lower WA percentages as compared to neat PC (Mix A), while Mix D showed comparable or slightly higher value after 28 days; (3) incorporation of CFs NPs within the PC–AAS pastes induced the reduction in TP%, which caused declines in

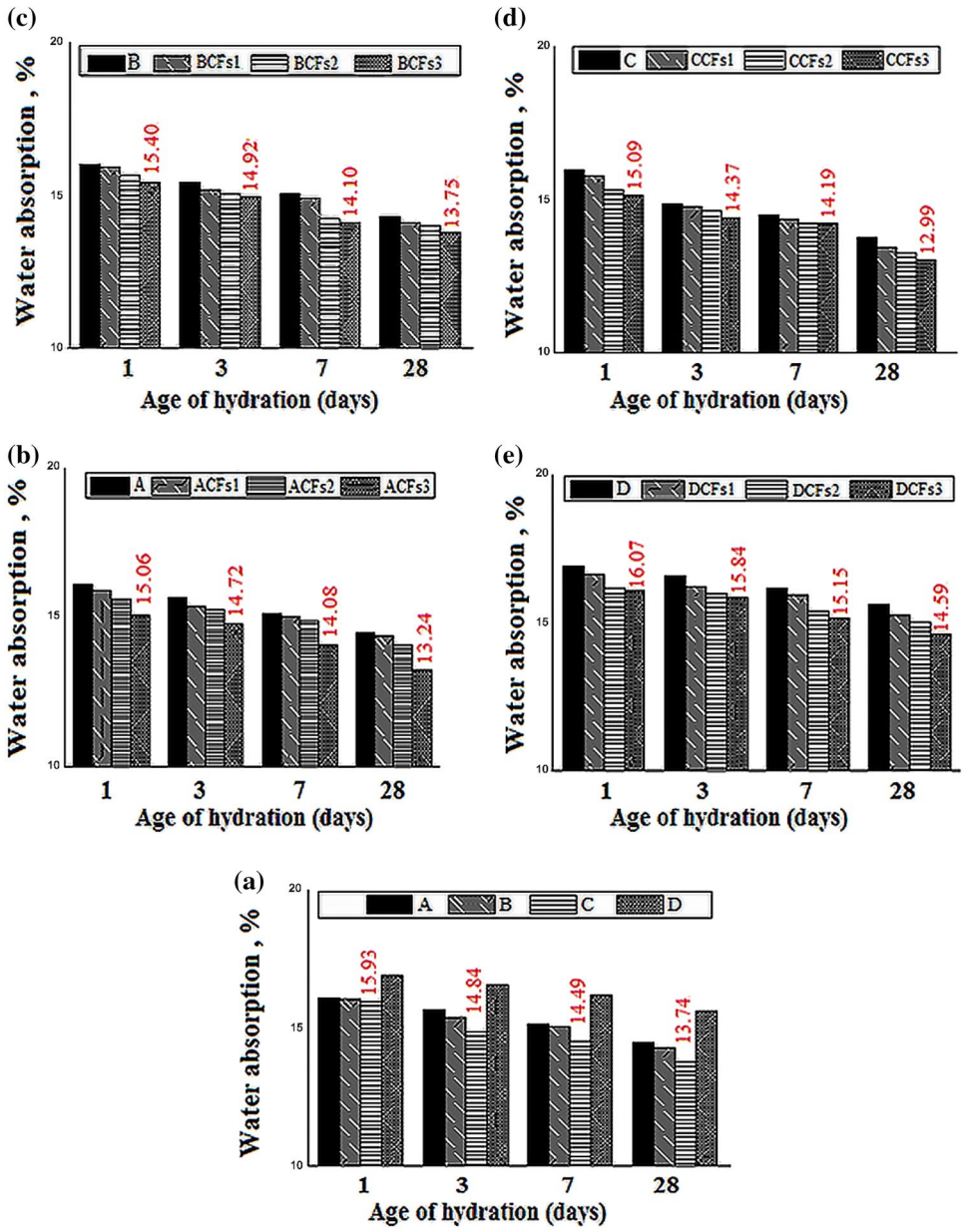

Fig.10 Water Absorption values of different hardened cement composites

the water absorption values for all prepared nanocomposites, and (4) the declining effect of CFs increased with its incorporation content along with the composite matrix from 1 to 28 days, and the WA values decreased (Fig. 10b–e). These outcomes agreed with the results of CS, BD, and TP results; the explanation of these outcomes has been mentioned previously.

The finding of CS, BD, TP, and WA tests shows that the nanocomposite 90PC–10AAS–2CFs has the optimum composition for application, as it presents optimum physical characteristics compared to all tested mixes during nearly all testing periods (86.94 Mpa, CS; 2.33 g/cm^3, BD; 35.12%, TP; and 12.99%, WA after 28 days of hydration).

Thermal resistivity (TR)

The influence of exposing the hardened composites made from (PC, PC–AAS, and PC–AAS–CFs) hydrated for 28 days to higher temperatures (300, 600, and 800 °C) was investigated. The CS values for different composites after firing at different temperatures for 3 h duration and left for slow cooling in air are graphically represented in Fig. 11a–d.

The main findings obtained are: (i) all composites showed a marked increase in the CS values upon heating up to 300 °C compared to their recorded values after 28 days of hydration, followed by a notable diminishing upon heating to 600 and 800 °C, (ii) all PC–AAS composites showed higher compressive strength values compared to that of neat PC cement (Mix A) at all testing temperatures, (iii) all composites admixed with CFs showed higher CS values compared to their controls (Mixes A–D) after firing at different temperatures, and (iv) as the amount of CFs increase the firing resistance increases (Figs. 11a–d). These outcomes could be explained as follows: the high upgrading in the CS values after exposure to 300 °C could be credited to the hydrothermal reaction (internal autoclaving) that occurs between the H_2O vapor molecules generated from the evaporation of physically adsorbed water inside different pores along with the hardened cement matrix and the residual unreacted cement grains [27]. The obvious enhancement in the thermal stability of different nanocomposites (especially Mix DCFs3) at 300 °C is assigned to the perfect dispersion of CFs NPs within the composite matrix and its effectiveness to induce the formation of large quantities of various hydration products via its nucleation effect and activation of the internal autoclaving. These products are stuck in the available spaces (macro and micropores) along the hardened composite, promoting the formation of the hardened matrix that has good resistance to fire deterioration [28]. Evidently, the noticed decrease in the CS values for all composites upon exposure to 600 °C is mainly ascribed to the thermal degradation of nearly all fundamental products such as CSH (I and II), CAH, CASHs, AFm, Aft, CFSH, and CH [27]. Finally, the enormous depletion in CS values for all tested

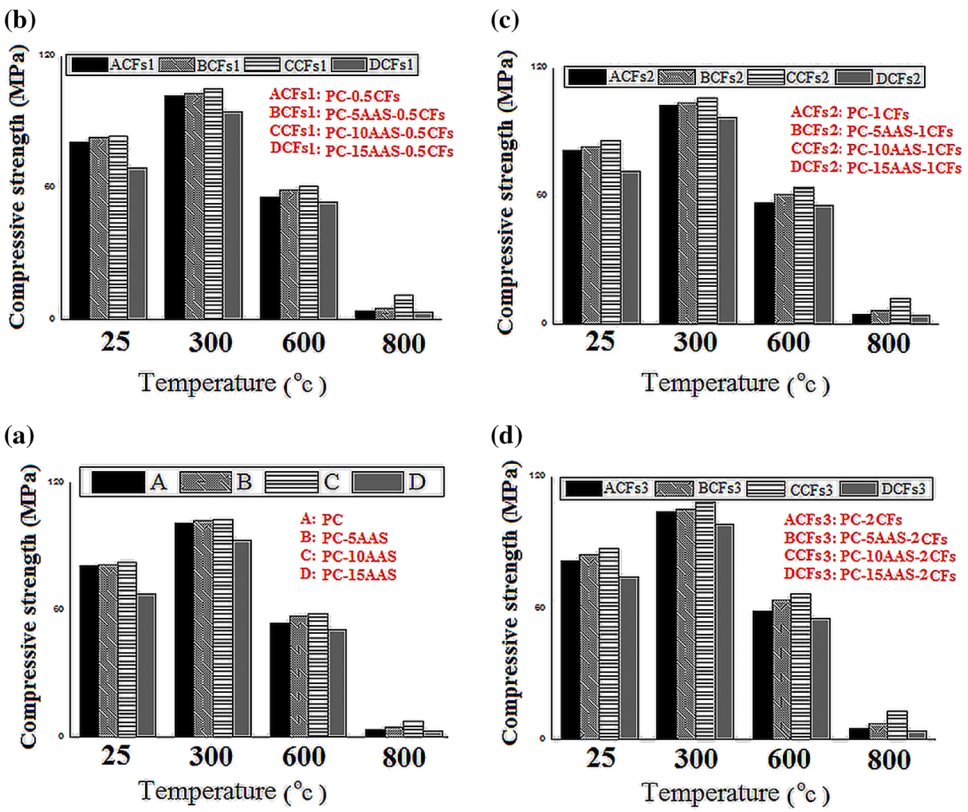

Fig. 11 Compressive strength values for different fired cement composites after slow cooling in air

composites after firing at 800 °C is assigned to the complete thermal degradation for all binding centers, as well as the induction of several cracks along with the composite matrix [18].

The CS values for different composites after exposure to 300, 600, and 800 °C for 3 h and cooled suddenly (by cold water) are represented in (Fig. 12a–d). Clearly, the CS values for these composites are lower than their analogs fired at the same temperatures and cooled in the air (slowly). Also, all composites showed a continuous deterioration in CS with increase in the firing temperature (from 300 up to 800 °C) (Fig. 12a–d). The significant reduction in CS is ascribed to the formation of several cracks as well as enlargement of the already generated crack (micro-cracks induced during the firing) because of the thermal shock that occurred during the rapid cooling process [24]. All examined composites show a continuous notable depression in the compressive strength with increase in the heating temperature from 300 to 600 °C and then reached zero at 800 °C. However, the degree of loss in strength in the case of blended samples with or without CFs NPs is higher than that of neat Portland cement pastes with or without CFs NPs.

Figure 13a–d demonstrates the percentage relative compressive strength (RCS) (relative to their CS after 28 days) for all fired specimens after some time. The calculated RCS percentages values are 125.16, 125.4, 125.53 and 128.79 for Mixes A–D, respectively, 125.26, 125.31 and 125.43 for Mixes ACFs1–ACFs3), respectively, 125.46, 125.58 and 125.61 for Mixes BCFs1–BCFs3, respectively, 126.37, 126.39 and 126.41 for Mixes CCFs1–CCFs3, respectively, and 134.81, 135.22 and 136.07 for Mixes DCFs1–DCFs3, respectively, after firing at 300°C and cooled slowly (Fig. 13ad). Evidently, these findings show the nanocomposite containing 85% PC–15% AAS waste–2% CFs to be the best selection for thermal application, as it presents the highest residual strength (highest % RCS), which is a perfect result from the economic and environmental point of views.

Figure 14a–d displays the percentage relative compressive strength (relative to their CS after 28d) for different composites after firing and rapid cooling. The RCS% values for these composites after firing at 300 °C and rapidly cooled are 95.17, 95.29, 95.79 and 91.12 for Mixes A–D, respectively, 96.75, 97.45 and 97.62 for Mixes ACFs1–ACFs3, respectively, 96.77, 97.51, and 97.63 for Mixes BCFs1–BCFs3); respectively, 96.85, 97.54 and 97.99; (Mixes CCFs1-CCFs3, respectively, and 96.12, 96.59 and 97.60 for Mixes DCFs1–DCFs3, respectively. These finding support the positive impact of CFs on upgrading the fire resistance for different PC–AAS blended pastes.

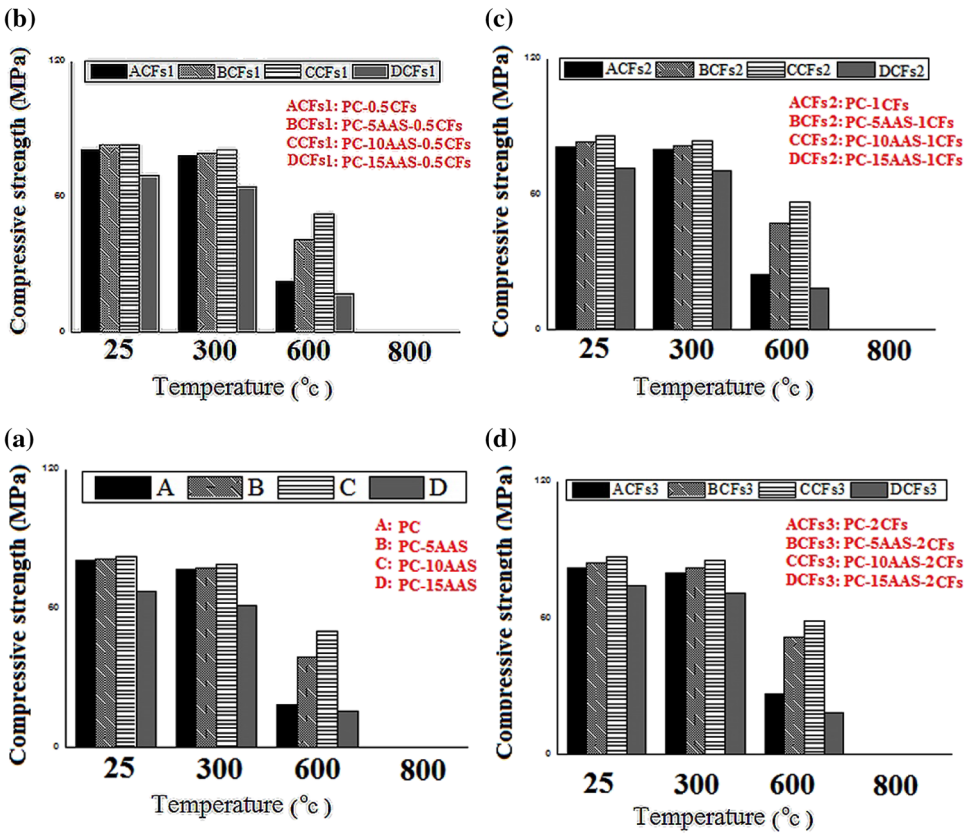

Fig. 12 Compressive strength values for different fired cement composites after suddenly cooling

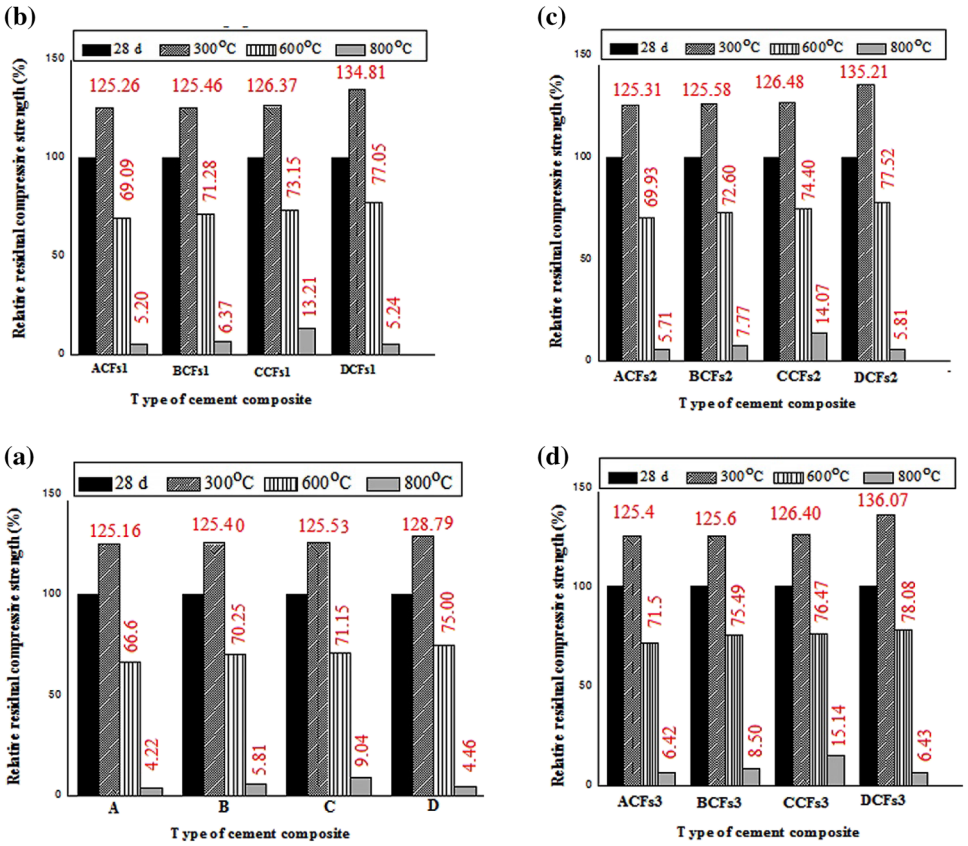

Fig. 13 Relative residual compressive strength values for different fired cement composites after slow cooling in air

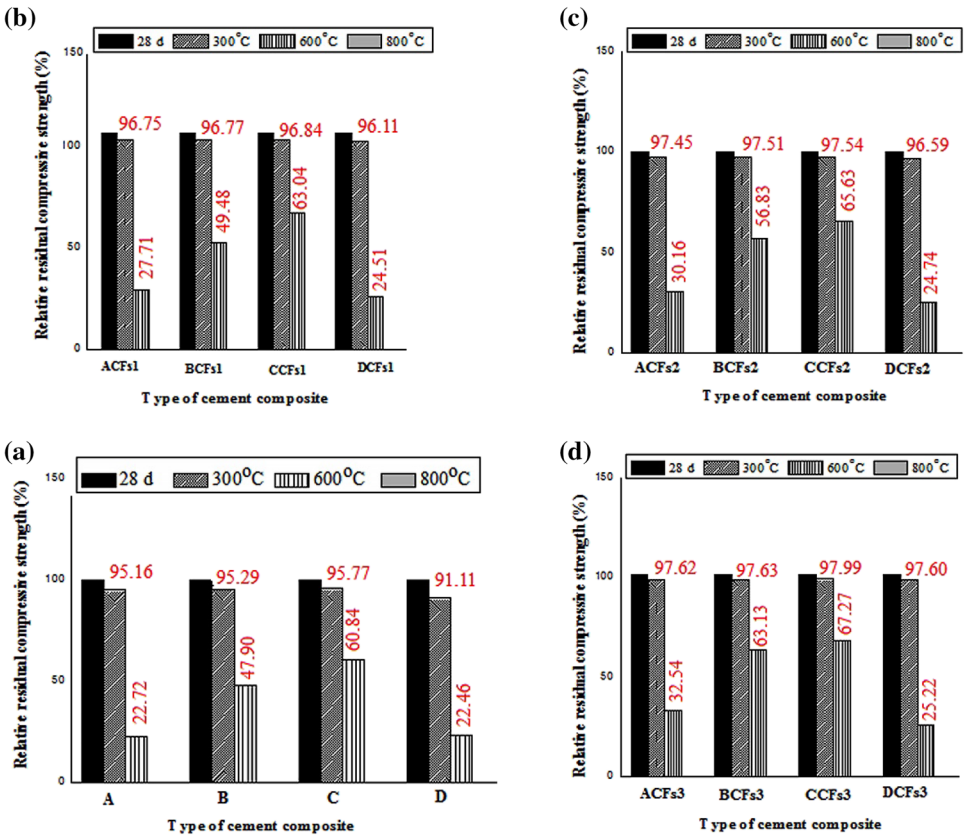

Fig. 14 Relative residual compressive strength values for different fired cement composites after suddenly cooling

Phase composition

X-ray diffraction (XRD)

The XRD patterns of composites made from 100 PC, 95PC–5AAS, 90PC–10 AAS, PC–2 CFs, 95PC–5AAS–2 CFs and 90 PC–10 AAS–2CFs after 7 and 28 days of hydration are displayed in Figs. 15 and 16, respectively. The main indication of the XRD patterns is the formation of CSH and CH as major products, as their characteristic peaks appeared in XRD patterns of all mixes [29] (Fig. 15). The indicative peaks of unreacted portion C_3S, β-C_2S, and quartz could also be distinguished. Besides, the peaks characteristic of the calcite phase ($CaCO_3$) is also identified, due to the reaction of the created lime (CH) with atmospheric CO_2 gas [30]. The inclusion of 2% CF NPs along these composites (Mixes ACFs3, BCFs3, and CCFs3) induced the formation of extra amounts of CAH, CASH, CSH (I), and CSH (II). Besides, $CuFe_2O_4$

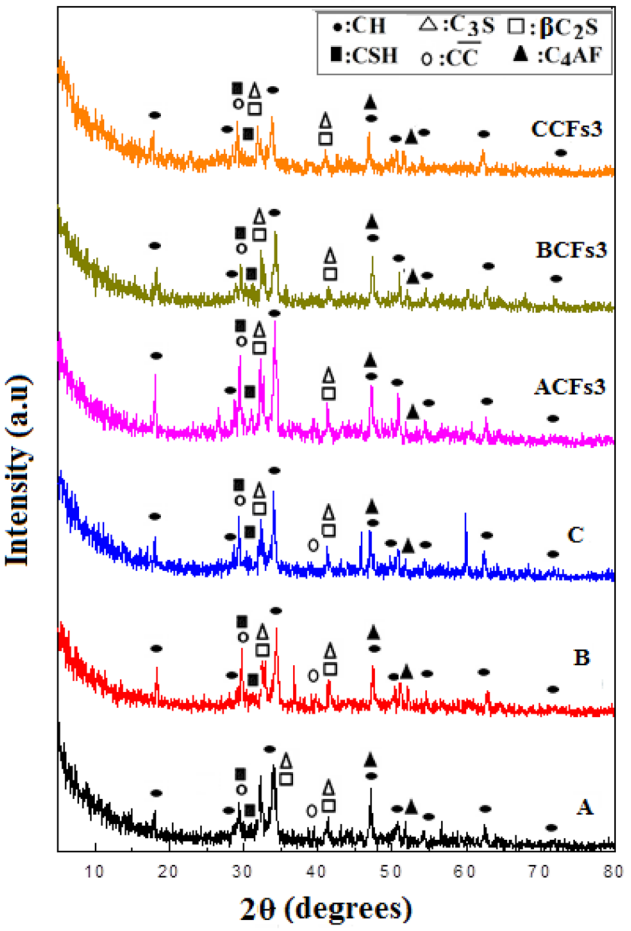

Fig. 15 XRD patterns of hardened composites made from (Mix A–C), and nanocomposites made from (Mix ACFs3–CCFs3) at 7 days of hydration

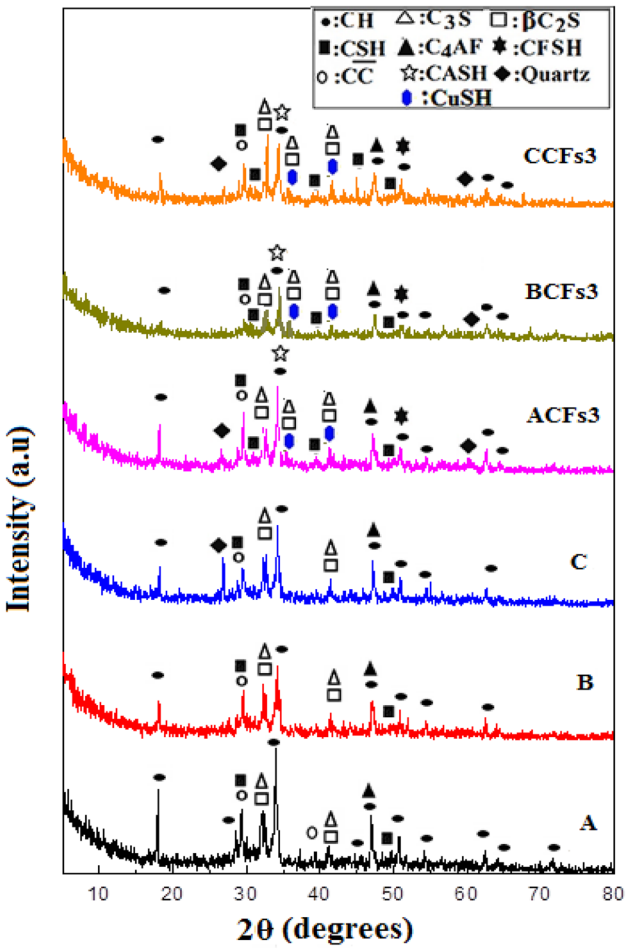

Fig. 16 XRD patterns of hardened composites made from Mixes (A–C), and nanocomposites made from Mixes (ACFs3–CCFs3) at 28 days of hydration

nanoparticles dissociate and undergo a pozzolanic reaction with $Ca(OH)_2$ liberated from clinker hydration causing the creation of new phases, namely ilvaite, $CaFe^{2+}Fe^{3+}Si_2O_7O(OH)$, (CFSH) and CuSH. The indicative peaks of these products are well displayed in the patterns. The accumulation of these products is contributed strongly to the development of compressive strength. The XRD analysis supports the previously reported CS results, which revealed that the nanocomposites presented high mechanical characteristics (high CS) than their controls (composites without CFs NPs). Evidently, the XRD pattern is a qualitative technique as it detects only the crystalline portion of any material. So, it can be used to detect the phase change during the progress of the hydration process or by the addition of different admixtures as nanomaterials. Figure (16) display the XRD patterns of selected samples after 28 days; clearly, the same phases were identified for all tested samples.

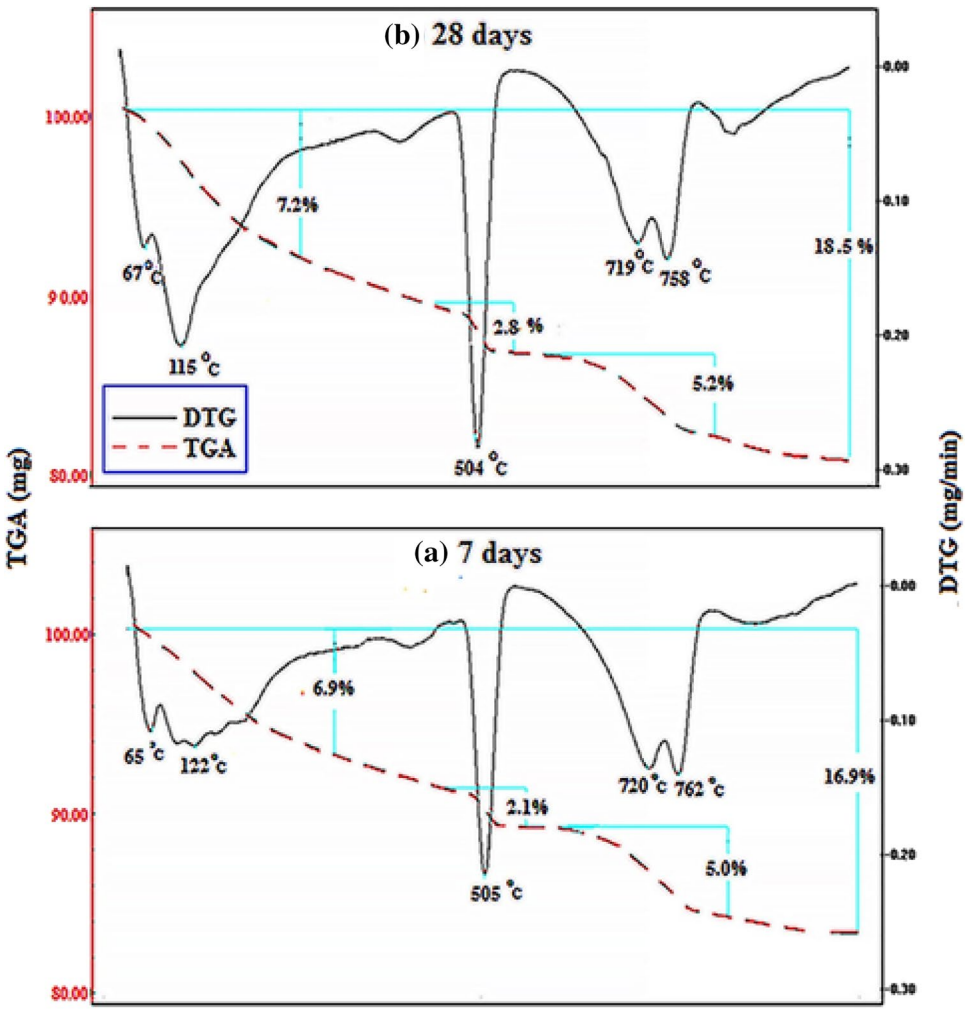

Fig. 17 TG/DTA thermograms of hardened neat PC pastes (Mix A) at (**a**) 7 days and (**b**) 28 days of hydration

Differential thermogravimetric analysis

Figures 17, 18, 19, and 20 illustrate the differential thermogravimetric analysis (TG/DTA) obtained for PC, PC–2CFs, PC–10 AAS and PC–10 AAS–2 CFs (Mixes A, ACFs3, C and CCFs3, respectively) after 7 - and 28 days of hydration. Figure 17a, b indicates the presence of four endothermic peaks at temperature zones of ~ 70–180, ~ 505 0.720, and 760 °C, for neat PC sample hydrated for 7 and 28 days, respectively. The first endothermic peak presented at the range of 70–180 °C refers to the removal of physically adsorbed (nonbounded water) as well as the amorphous parts of CSHs, ettringite ($3CaO.Al_2O_3.3CaSO_4.32H_2O$), and monosulfate ($3CaO.(Al,Fe)_2O_3.CaSO_4.nH_2O$) [31] after 7 and 28 days of hydration, respectively. The endothermic peak located at 505 °C, is assigned to the thermal destruction of $Ca(OH)_2$ [32, 33]. The % mass loss of the first peak is 6.9 and 7.2, while for the second peak 2.1 and 2.8 after 7 and 28 days of hardening, respectively. These values affirmed the development of the hydration process of PC and the formation of extra quantities of CSHs, ettringite, and AFm (monosulphate), and CH as the main hydration products [27]. The presence of double peaks appearing at 720 and 760 ascertain the partial carbonation of the formed hydration products during the handling of the specimens. The double peaks account for the existence of carbonates with different degrees of crystallinity, and the values of the percentage mass loss of these peaks are correlated to the degree of crystallinity as well as the degree of carbonation [29].

Figure 18a and b displays the TG/DTA data of PC–2CFs nanocomposite (Mix ACFs3). The TG/DTA results of this composite are identical with that of neat PC (Mix A), but with a notable increase in the %total mass loss (especially for peaks present at ~ 70–180 °C and ~ 506 °C). The entire % mass reduction of the diverse hydration yields are 16.9 to 18.5% (for PC) and 17.5, 18.9 (for PC–2% CFs) after 7 and 28 days, respectively. This finding is due to the catalytic acceleration effect of CFs NPs that act as nucleation centers for the hydration process to create additional supplemental hydration products, which participate in mechanical aspects of boosting. The TG/DTA data

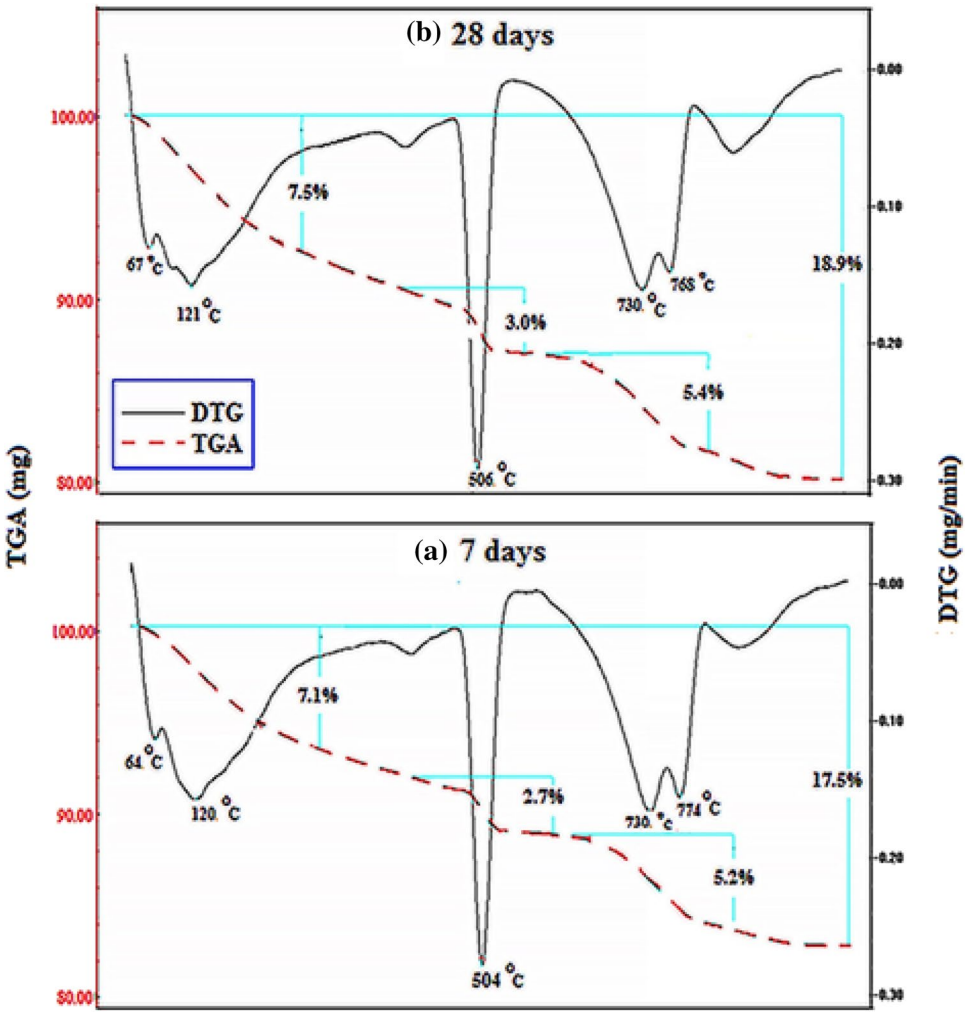

Fig. 18 TG/DTA thermograms of hardened neat PC pastes containing 2% CFs NPs (Mix ACFs3) at (**a**) 7 days and (**b**) 28 days of hydration

agreed with the compressive strength results mentioned previously in this study.

Figure 19a and b demonstrates the TG/DTA thermograms of the hardened specimens made from PC–10 AAS (Mix C). The same main endothermic peaks, as well as the same behavior as neat PC (Mix A), are observed. The values of mass loss (%) of the first peak (at ~ 70–180 °C) are 7.0 and 7.1, while the value for the second endothermic peak (at about 505 °C) is 2.2–2.9 after 7–28 days, respectively. These values are correlated to both the quantity and the degree of crystallinity of the formed products. The peak detected at ~ 740 °C is referred to as the decomposition of different carbonates formed as a result of specimen carbonation during handling processes. Obviously, the total % mass losses for all the formed products are 18.2 and 19 after 7 and 28 days, respectively, which are higher than that of neat PC (16.9 and 18.5). The notable increase in the percentage of total mass loss is correlated to the formation of extra amounts of nearly amorphous and illcrystalline CSH as the main hydration product, formed from the pozzolanic reaction between CH, liberated from PC hydration, and amorphous silica and alumina phases present in AAS waste. These findings are corroborated with the compressive strength results.

Figure 20a and b displays the TG/DTA curves for PC–10 AAS–2.0 CFs nanocomposite (Mix CCFs3) after 7- and 28-day hydration. This nanocomposite shows the same peaks as in the case of the PC–10AAS composite. The first endothermic peak found at 70–180 °C referred to the removal of evaporable water and decomposition of CSH and sulfoaluminates in addition to the thermal ruptures for secondary hydration yields such as gehlenite hydrate (C_2ASH_8) and hydrocalumite (C_4AH_{13}), and the mass loss% for this peak is 6.9 and 7.8 after 7 and 28 days of hydration, respectively. The mass loss% for the second endothermic peak characteristic for decomposition of CH (located at ~ 500 °C) is 2.4 and 3.1 after 7 and 28 days, respectively. The observed increase in the mass loss% values of these two peaks is explained in terms of the continuity of the hydration reaction. It is observed from the figure that the total mass reduction percentages are 18.6 and 19.3% after 7 and 28 days, respectively, and these percentages are relatively higher when matched with the corresponding data of all tested specimens

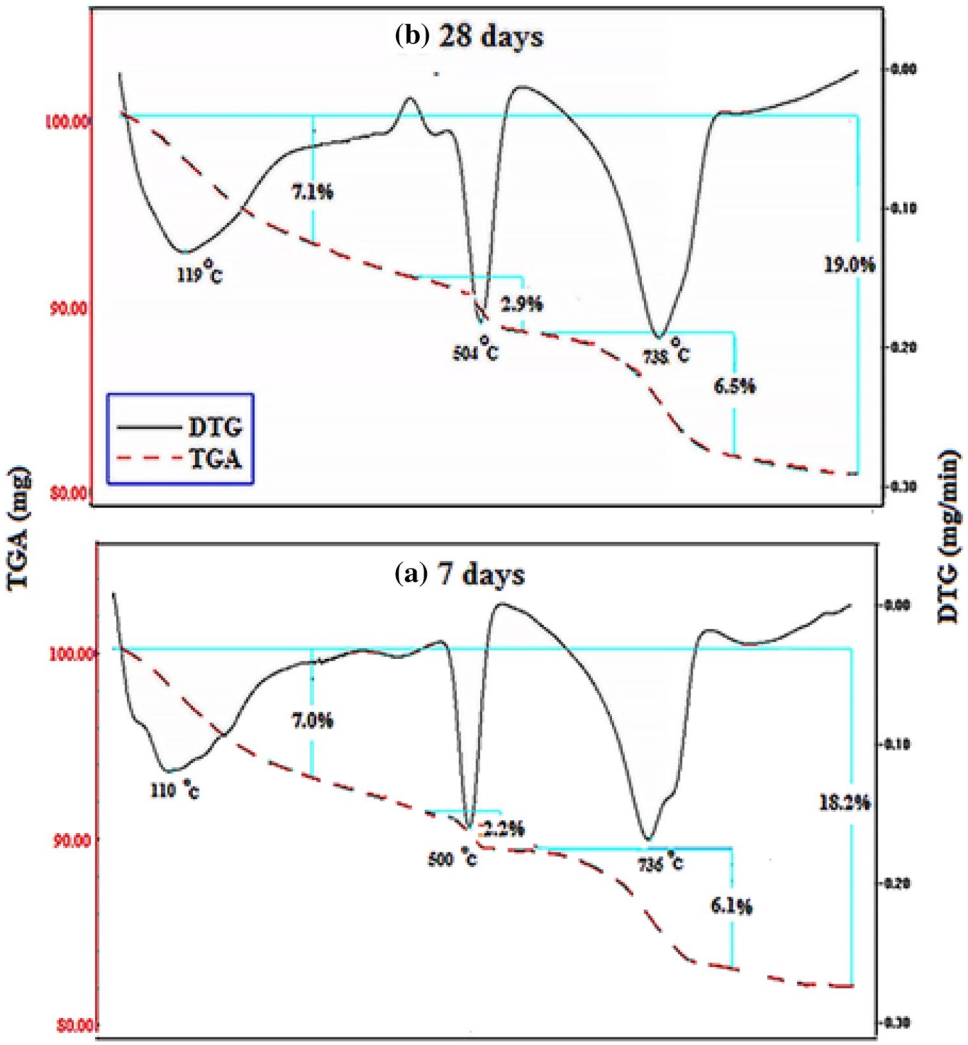

Fig. 19 TG/DTA thermograms of hardened blended specimens made from PC–10%ASAA (Mix C) (**a**) 7 days and (**b**) 28 days hydration

(Mixes A, ACFs3, C, and CCFs3). The notable increase in %total mass loss of these nanocomposites is ascribed to the reinforcing effect of the dispersed CFs NPs as mentioned previously. Also, the TG/DTA results agreed with all previously mentioned results (CS, TP, BD, and WA).

Morphology and textural characteristics

The morphology and the textural characteristics for Mix A specimens treated for 7 and 28 days are presented in Fig. 21a and b, respectively. After 7 days, the SEM images reflect the formation of the noncompact matrix and along with it some pores and a small amount of hydration products, mainly as CSH with illcrystalline and fibrous structure can be detected. Also, small amounts of CH as hexagonal plates dispersed along with the matrix and a small amount of calcite, besides a large amount of unreacted clinker grains can be well distinguished (Fig. 21a). After 28 days, the SEM image displayed a dense matrix composed of excessive amounts of microcrystalline and fibrous CSH as well as CH that displayed as stacked hexagonal crystals. Also, a very small amount of calcite can be observed in the matrix due to the side reaction of CO_2 with CH formed during handling of the sample (Fig. 21b). Besides, there are void spaces still present in the matrix available for the deposition of new hydration products.

Figure 21c displays the morphology of the hardened samples of Mix A exposed to firing at 300 °C, followed by slow cooling in air. The SEM images reflect the presence of a compact structure possessing a large amount of nearly amorphous fibrous C–S–H as the major hydration products interlocked with the hexagonal plates of CH. These microstructure features confirm the internal autoclaving reaction of unreacted PC grains that leads to the formation of an extra amount of hydration products (CSH, CH, CAHs, CASHs), promoting the formation of a dense structure with good mechanical characteristics (high CS values). This outcome agrees with the obtained data of CS, BD, TP, and WA results. The microstructure obtained for the PC specimen (Mix A), exposed to a higher temperature (800 °C) and

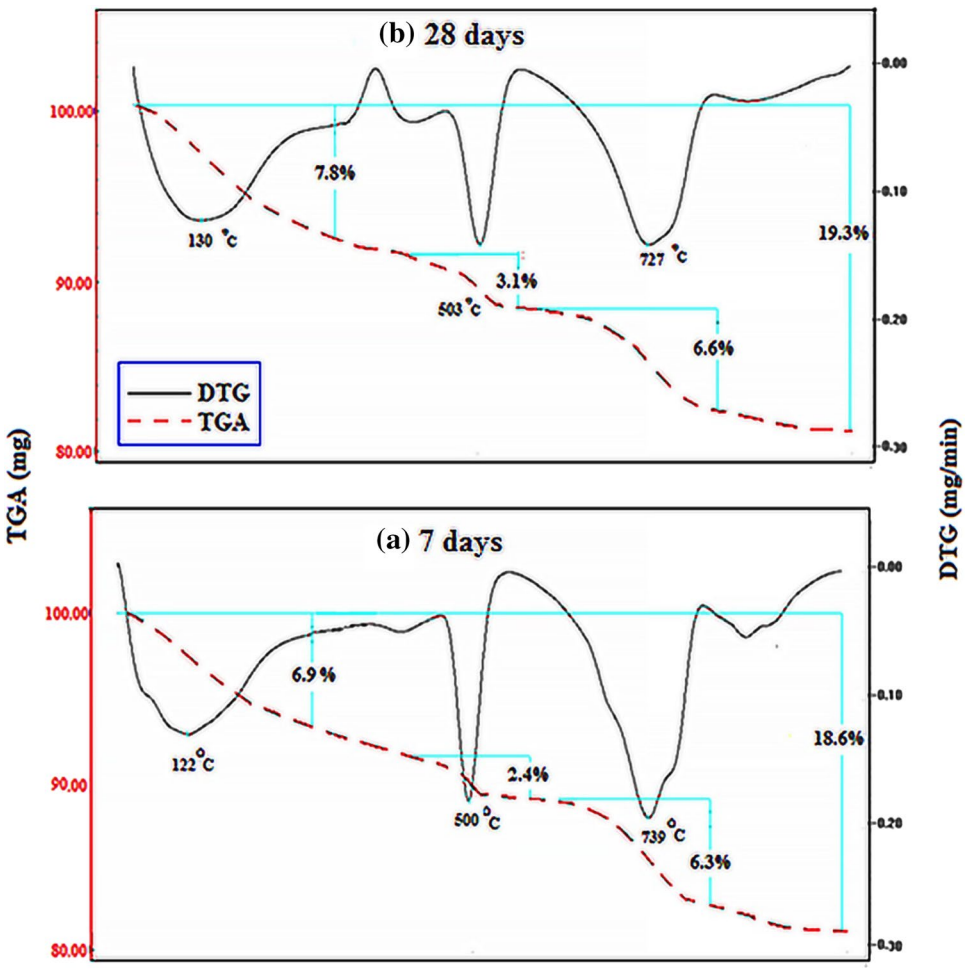

Fig. 20 TGA/DTG thermograms of hardened specimens made from PC–10%ASAA–2% CFs NPs (Mix CCFs3) at (**a**) 7 days and (**b**) 28 days of hydration

gradual cooling, illustrates the presence of several micro-cracks, and no hydration product could be distinguished since nearly all of them were decomposed. Certainly, the decomposition of the formed hydration products and the formation of micro-cracks are the main factors that cause the deterioration of these specimens. The very low CS values presented by these specimens agreed with the obtained SEM data (Fig. 21d).

Figure 22a and b represents the SEM images of hardened specimens made from 90 PC + 10AAS + 2 CFs (Mix CCFs3) after 7 and 28 days, respectively. The findings of the SEM micrographs of these nanocomposites are: (1) The SEM image of the specimen after 7 days is less dense and contains less amount of hydration products and a great part of unreacted clinker grains compared to its SEM image after 28 days of hydration. (2) Replacing PC with 10% AAS induces the formation of excess amounts of hydration products (namely, CSH, CAH, CASH), and all these products enhance the microstructure and the mechanical characteristics of these nanocomposites after 7 and 28 days compared to that of neat PC as indicated by the SEM images of this nanocomposite (Fig. 22a and b). (3) SEM micrographs of these specimens ascertain the filling effect of the nanoparticles to the existing pores as well as activation rule of CFs NPs, as it causes the formation of excessive products as its rule as active site and via its reaction and formation of a diverse product that appeared in the micrographs like; micro rods and fibrous crystals of CSHs, plates of CASHs, fine crystals of CFSH, CuSH and fibers of AFt ($3CaO{\cdot}Al_2O_3{\cdot}3CaSO_4{\cdot}32H_2O$); all formed hydration products are diffused with little hexagonal crystals of CH. The formation of additional hydration products and/or the formation of new products (CFSH and CuSH) is the main factor for the obtained dense and hard matrix for this nanocomposite Fig. 22a and b [27].

Figures 22c and d displays the SEM images of specimens made from Mix CCFs3 after firing at 300°C and 800°C and cooling in air. The images revealed microstructure upturn for these nanocomposites, which correlates with the rule of both AAS and CFS NPs. Figure 22c displays the SEM images of CCFs3 hardened sample fired at 300 °C and slowly cooled in air. The SEM images reflect the presence of a highly compact structure compared to the neat cement (Mix A) exposed to the same conditions, and the micro composition of this composite revealed

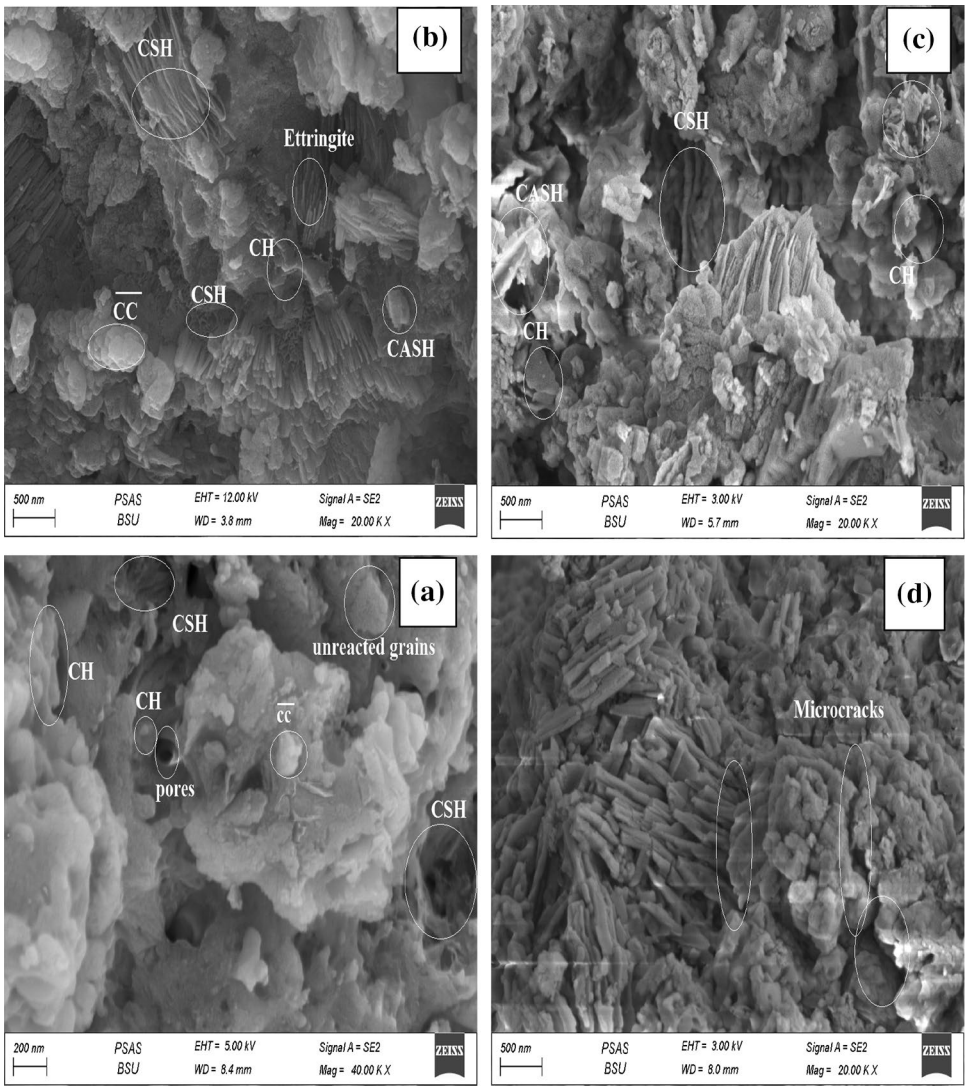

Fig. 21 SEM micrographs of PC-hardened cement pastes (Mix A): (**a**) after 7 days, (**b**) after 28 days, (**c**) after firing at 300 °C and (**d**) after firing at 800 °C

the existence of an excess amount of nearly amorphous fibrous C–S–H as the major hydration products, diffused with few hexagonal plates of CH. Also, some plates of CAHs, CASHs as well as fine crystals of CFSH and CuSH could be distinguished along the matrix. The formation of these products (especially fine crystals of CFSH and CuSH that fill up the micropores and mesopores of the hardened paste) promoted the formation of a dense structure with good mechanical characteristics (high CS values). The microstructure obtained for specimen made from Mix CCFs3, exposed to firing at 800 °C for 3 h and gradual cooling, revealed the complete decomposition of nearly all formed products, simulating the formation of micro-cracks and less dense and porous microcomposition. Clearly, the existence of CFs nanoparticles reduces the degree of porosity of the fired specimens when compared to neat cement (Mix A) exposed to the same condition (Fig. 22d).

Conclusion

The effect of the addition of small ratios of $CuFe_2O_4$ spinel nanoparticles on the physical, mechanical, microstructure, and deterioration characteristics of eco-friendly blended composites prepared from PC and AAS waste were investigated in this article. The main findings of this investigation can be summarized as follows:

1. The obtained results of all performed tests indicated the suitability of utilization of PC–AAS waste composite as an eco-friendly construction material.
2. Partial replacing of PC by AAS waste up to 10 mass% boosts the physicomechanical properties (CS, TP, BD, and WA %) of the hardened composites, while replacing

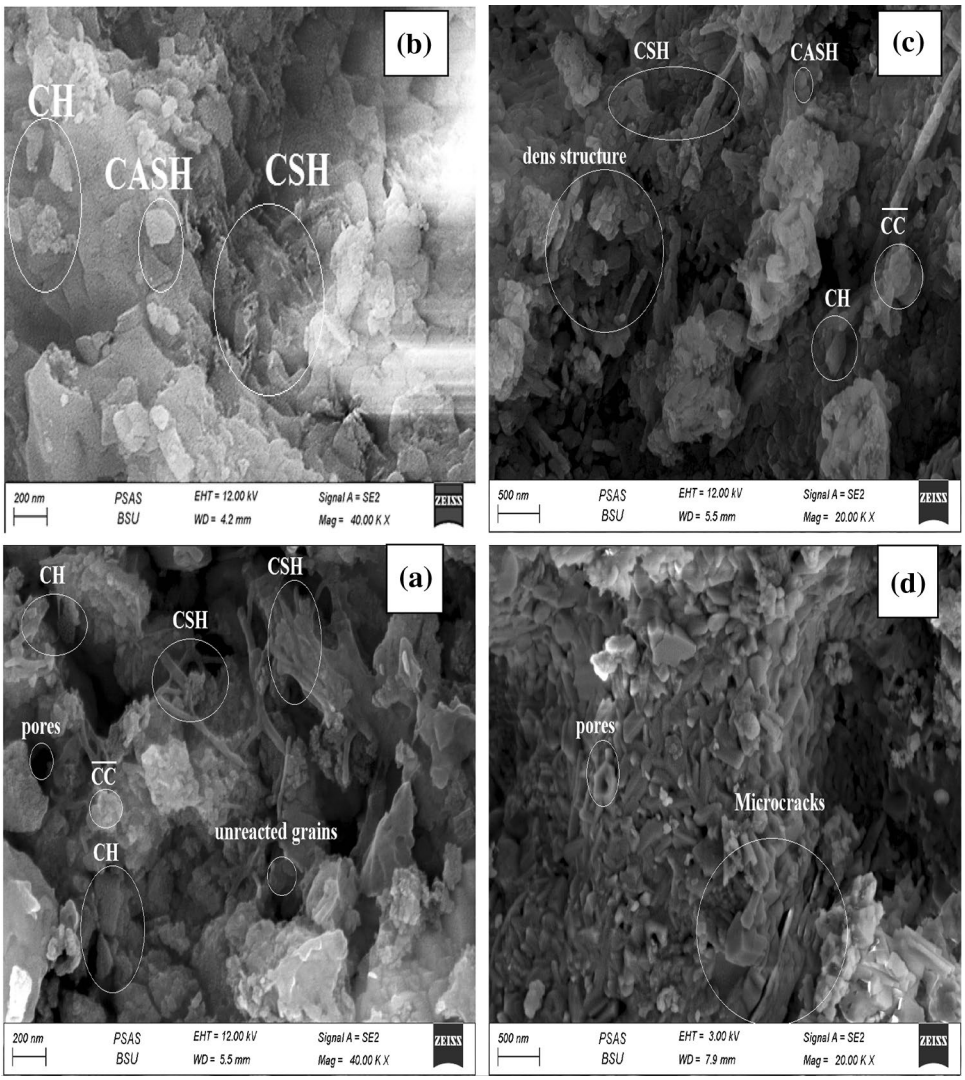

Fig. 22 SEM micrographs of PC-hardened cement pastes (Mix CCFs3): (**a**) after 7 days, (**b**) after 28 days, (**c**) after firing at 300 °C and (**d**) after firing at 800 °C

PC by 15% AAS waste has no enhancing effect on its physical and mechanical properties.

3. Inclusion of $CuFe_2O_4$ spinel nanoparticles up to 2 mass% in PC pastes blended with different ratios of AAS waste motivates the formation of hardened nanocomposites with improved physicomechanical characteristics and thermal stability.
4. The results affirmed that 90% PC–10% AAS waste–2% CFs composite could be considered the optimum choice for general construction application, as it displayed the highest CS values as compared to all other tested nanocomposites at almost all ages of hydration.
5. From the economic and environmental point of view, composite containing 90 PC–10 AAS–2 CFs offers many benefits, as replacement of PC by 10% AAS helps in reducing waste disposal costs (landfill tax), offering an alternative use for recycled water-treated plant sludge, without prejudging on either cost or quality, as well as protecting the environment by saving energy and diminishing the amount of harmful gases (CO_2 and NO_x) and other air pollutants emitted from the cement industry.
6. Nanocomposite with composition 85% PC–15% AAS waste–2% CFs presents the best thermal stability (highest RCS%), and is considered a perfect result from the economic and environmental point of view to use this nanocomposite for construction exposed to high temperatures.
7. TGA/DTG and XRD techniques affirmed the catalytic activity of $CuFe_2O_4$ spinel NPs, as they demonstrated the presence of an excessive amount of CSHs, AFt, AFm, CASHs, CAHs, CuSH, and CFSH in the presence of these NPs.
8. The SEM images affirmed that inclusion of 2% CFs NPs in PC–10 AAS composite during exposure to elevated temperature (300 °C) reinforced its microstructure and mechanical characteristics via promoting the formation of excessive amounts of diverse hydration products

as CSHs (I and II) as rod crystals, fibers of ettringite, plates of CASHs, hexagonal sheets of CH and CuSH gels. However, upon firing at 800 °C, thermal degradation for most hydration products and micro/micro-cracks appeared but with less extent compared with neat PC.

Funding Open access funding provided by The Science, Technology & Innovation Funding Authority (STDF) in cooperation with The Egyptian Knowledge Bank (EKB).

Declarations

Conflict of interest The authors declare that there are no known conflicts of interest associated with this publication and there has been no significant financial support for this work that could have influenced its outcome.

References

1. He ZH, Yang Y, Yuan Q, Shi JY, Liu BJ, Liang CF, Du SG (2021) Recycling hazardous water treatment sludge in cement-based construction materials: Mechanical properties, drying shrinkage, and nano-scale characteristics. J Clean Prod 290:125832
2. Kaur G, Pavia S (2021) Chemically treated plastic aggregates for eco-friendly cement mortars. J Mater Cycles Waste Manage 23:1531–1543
3. Pavesi TB, Rohden AB, Garcez MR (2021) Supporting circular economy through the use of red ceramic waste as supplementary cementitious material in structural concrete. J Mater Cycles Waste Manage 23:2278–2296
4. Owaid HM, Hamid R, Taha MR (2019) Durability properties of multiple-blended binder concretes incorporating thermally activated alum sludge ash. Constr Build Mater 200:591–603
5. Liu Y, Zhuge Y, Chow CWK, Keegan A, Pham PN, Li D, Oh JA, Siddique R (2021) The potential use of drinking water sludge ash as supplementary cementitious material in the manufacture of concrete blocks. Resour Conserv Recy 168:105291
6. Dahhou M, El Moussaouiti M, Arshad MA, Moustahsine S, Assafi M (2018) Synthesis and characterization of drinking water treatment plant sludge-incorporated Portland cement. J Mater Cycles Waste Manage 20:891–901
7. Dubey S, Agarwal M, Gupta AB (2019) Use of waste sludge generated from water defuoridation plant as partial substitute for fne aggregates in mortars: microstructural characterization and compressive strength. J Mater Cycles Waste Manage 21:1526–1540
8. Abo-El-Enein SA, El-Hosiny FI, El-Gamal SMA, Amin MS, Ramadan M (2018) Gamma radiation shielding, fire resistance and physicochemical characteristics of Portland cement pastes modified with synthesized Fe_2O_3 and ZnO nanoparticles. Constr Build Mater 173:687–706
9. Magnago RF, TdeA B, de Aguiar AC, Baungarten P, Mendonça BAB, Silva HRT, Egert P, Girotto E, Júnior AC, Parma GOC (2021) Recycling glass-polishing sludge and aluminum anodising sludge in polyurethane and cement composites: fire performance and mechanical properties. J Mater Cycles Waste Manage 23:1126–1140
10. Xiao H, Zhang F, Liu R, Zhang R, Liu Z, Liu H (2019) Effects of pozzolanic and nonpozzolanic nanomaterials on cement-based materials. Constr Build Mater 213:1–9
11. Reches Y, Thomson K, Helbing M, Kosson DS, Sanchez F (2018) Agglomeration and reactivity of nanoparticles of SiO_2, TiO_2, Al_2O_3, Fe_2O_3, and clays in cement pastes and effects on compressive strength at ambient and elevated temperatures. Constr Build Mater 167:860–873
12. Meng W, Khayat KH (2018) Effect of graphite nanoplatelets and carbon nanofibers on rheology, hydration, shrinkage, mechanical properties, and microstructure of UHPC. Cem Concr Res 105:64–71
13. El-Gamal SMA, Hashem FS, Amin MS (2017) Influence of carbon nanotubes, nanosilica and nanometakaolin on some morphological-mechanical properties of oil well cement pastes subjected to elevated water curing temperature and regular room air curing temperature. Constr Build Mater 146:531–546
14. Kamal M, Safan MA, Eltabey M, ElS Z, Abu El-hassan KH (2012) Compressive strength of Portland cement pastes and mortars containing Cu-Zn nano-ferrite. Int J Nano Dimens 3(2):91–100
15. Jiao D, El Cheikh K, Shi C, Lesage K, De Schutter G (2019) Structural build-up of cementitious paste with nano-Fe3O4 under time varying magnetic field. Cem Concr Res 124:105857
16. TS 25 (2008) Natural pozzolan (Trass) for use in cement and concrete definitions, requirements and conformity criteria. Turkish Standards Institute, Ankara, pp 1–14
17. Baki VA, Nayır S, Erdoğdu Ş, Ustabaş Ĺ (2020) Determination of the Pozzolanic activities of trachyte and rhyolite and comparison of the test methods implemented. Int J Civ Eng 18:1053–1066
18. Amin MS, El-Gamal SMA, Hashem FS (2015) Fire resistance and mechanical properties of carbon nanotubes–clay bricks wastes (Homra) composites cement. Constr Build Mater 98:237–249
19. Farghali AA, Khedr MH, Abdel Khalek AA (2007) Catalytic decomposition of carbondioxide over freshly reduced activated $CuFe_2O_4$ nano-crystals. J Mater Process Technol 181:81–87
20. Samson VAF, Bernadsha SB, Mahendiran M, Lawrence KL, Madhavan J, Raj MVA, Prathap S (2020) Impact of calcination temperature on structural, optical, and magnetic properties of spinel $CuFe_2O_4$ for enhancing photocatalytic activity. J Mater Sci Mater Electron 31:6574–6585
21. El-Gamal S, Selim F (2017) Utilization of some industrial wastes for eco-friendly cement production. Sustain Mater Technol 12:9–17
22. Ababneh FA, Alakhras AI, Heikal M, Ibrahim SM (2019) Stabilization of lead bearing sludge by utilization in fly ash-slag based geopolymer. Constr Build Mater 227:116694
23. El-Gamal SMA, Hashem FS, Amin MS (2012) Thermal resistance of hardened cement pastes containing vermiculite and expanded vermiculite. Therm Anal Calorim 109:217–226
24. El-Gamal S, Abo-El-Enein S, El-Hosiny F, Amin M, Ramadan M (2018) Thermal resistance, microstructure and mechanical properties of type I Portland cement pastes containing low-cost nanoparticles. J Therm Anal Calorim 131(2):949–968
25. El-Gamal SMA, El-Hosiny FI, Amin MS, Sayed DG (2017) Ceramic waste as an efficient material for enhancing the fire

resistance and mechanical properties of hardened Portland cement pastes. Constr Build Mater 154:1062–1078
26. Liu Y, Zhuge Y, Chow CWK, Keegan A, Pham PN, Li D, Oh JA, Siddique R (2020) The potential use of drinking water sludge ash as supplementary cementitious material in the manufacture of concrete blocks. Resour Conserv Recy 168:105291
27. Ramadan M, El-Gamal SMA, Selim FA (2020) Mechanical properties, radiation mitigation and fire resistance of OPC-recycled glass powder composites containing nanoparticles. Constr Build Mater 251:118703
28. Ramadan M, Amin MS, Sayed MA (2020) Superior physico-mechanical, fire resistivity, morphological characteristics and gamma radiation shielding of hardened OPC pastes incorporating $ZnFe_2O_4$ spinel nanoparticles. Constr Build Mater 234:117807
29. Amin M, El-Gamal S, Abo-El-Enein S, El-Hosiny F, Ramadan M (2015) Physicochemical characteristics of blended cement pastes containing electric arc furnace slag with and without silica fume. HBRC J 11(3):321–327
30. Habib A, Aiad I, El-Hosiny F, El-Aziz AA (2018) Development of the fire resistance and mechanical characteristics of silica fume-blended cement pastes using some chemical admixtures. Constr Build Mater 181:163–174
31. Abo-El-Enein SA, Hashem FS, Amin MS, Sayed DM (2016) Physicochemical characteristics of cementitious building materials derived from industrial solid wastes. Constr Build Mater 126:983–990
32. Abo-El-Enein SA, El-Gamal SMA, Aiad IA, Azab MM, Mohamed OA (2018) Early hydration characteristics of oil well cement pastes admixed with newly prepared organic admixture. HBRC J 14:207–214
33. Selim FA, Hashem FS, Amin MS (2020) Mechanical, microstructural and acid resistance aspects of improved hardened Portland cement pastes incorporating marble dust and fine kaolinite sand. Constr Build Mater 251:118992